

Article

Improvement of Methane Combustion Activity for Pd/ZrO₂ Catalyst by Simple Reduction/Reoxidation Treatment

Chansong Kim, Eunpyo Hong and Chae-Ho Shin * 

Department of Chemical Engineering, Chungbuk National University, Cheongju, Chungbuk 28644, Korea; cksth1210@naver.com (C.K.); love_blueangel@hanmail.net (E.H.)

* Correspondence: chshin@chungbuk.ac.kr; Tel.: +82-43-261-2376

Received: 20 September 2019; Accepted: 8 October 2019; Published: 10 October 2019



Abstract: The improvement of methane combustion activity was observed in cyclic temperature-programmed and isothermal reactions over Pd/ZrO₂ catalysts by simple reduction/reoxidation treatment. The catalytic activity increased during the initial stages of isothermal reaction, and the light-off temperature was lowered as the number of cycles increased in the cyclic temperature-programmed reaction. To reveal the origin of activation, variations in the reduction properties after the activation period were carefully investigated through CH₄ temperature-programmed reduction (TPR) measurements. From the CH₄-TPR results, it was confirmed that the reduction temperature decreased significantly after activation. The observation of the CH₄-TPR peak at relatively low temperatures is directly proportional to the catalytic activity of CH₄ combustion. It was therefore concluded that repeated reduction/reoxidation occurred in the reactant stream, and this phenomenon allowed the combustion reaction to proceed more easily at lower temperatures.

Keywords: CH₄ temperature-programmed reduction; methane combustion; Pd/ZrO₂ catalyst; reduction; calcination

1. Introduction

Methane is the main constituent of natural gas and is commonly employed as an energy resource. However, methane is the second largest contributor to global warming after carbon dioxide, and it has a global warming potential 21 times higher than the same mass of carbon dioxide [1]. Therefore, the efficient combustion of methane and its controlled emission is of importance in various industrial fields, such as natural gas-fueled vehicles, power plants, burners, boilers, and incinerators [2,3]. Catalytic methane combustion could therefore be considered a suitable alternative to conventional thermal oxidation, as it can minimize thermal NO_x generation due to its lower operation temperatures. Thus, the catalytic combustion of methane has been extensively studied using a range of catalysts including CeO₂ [4], Al₂O₃ [5–9], ZrO₂ [10–13], MgAl₂O₄ [2,14], NiAl₂O₄ [1,15], and SnO₂ [16] supported metal catalysts, and supported Pd catalysts are the most widely utilized to date.

The performance of catalysts in methane combustion is mainly considered in terms of activity and stability. More specifically, in terms of catalytic activity, it is important that the reaction can be initiated at relatively low temperatures. For example, in the case of vehicle emission control catalysts, the catalyst cannot participate in the combustion reaction until the temperature reaches the required operating temperature, and so lower reaction temperatures are favored. Similarly, the use of a low temperature ignition catalyst in gas turbines can avoid the necessity to preheat the reactant stream [15]. In this context, several studies have reported that the pre-reduction of a catalyst can improve its reactivity, in particular at low temperatures [6,12,17–20]. Although the PdO and PdO_x species in supported Pd catalysts can be pre-reduced, the resulting Pd⁰ species cannot be considered as active species, as it

subsequently transforms into PdO or PdO_x once again upon contact with the reactant stream. It therefore appears that reduction/reoxidation treatments can alter the physicochemical properties of such catalysts, including the reducibility [12], surface structure [20], and oxygen content [8,17,21], thereby enhancing their catalytic activities.

Stability is also important in determining the performance of a catalyst. Improving the hydrothermal stability of emission-control catalysts is essential, as exhaust gases contain large quantities of water vapor. Indeed, catalytic activities are known to gradually decrease with increasing time-on-stream, due to the thermal decomposition of PdO to metallic Pd⁰ [8,22,23] and due to thermal sintering [8,18,24,25]. In the presence of water vapor, water and methane competitively adsorb on the same active sites [25] and the water promotes the formation of surface Pd(OH)₂ species [5,13,26,27], which are less reactive towards hydrocarbon combustion. In addition, water adsorbed on the support can also hinder oxygen migration to the active site from the reducible support [5,28,29]. In contrast, the activation phenomenon, in which the conversion increases with time on stream, is often observed over Pd/ZrO₂ [11,21,30] and Pd/Al₂O₃ [6,8,20,30–32] catalysts. For example, Demoulin et al. [6] reported activation over Pd/γ-Al₂O₃, which resulted in an increased methane conversion from ~30%~80% over 30 h. They proposed that this activation phenomenon was caused by the removal of contaminants from the catalyst surface, sintering of the palladium phase, and structural changes. Although various hypotheses have been proposed, the mechanism of this activation phenomenon is not yet fully understood. However, the increased activity with time on stream is influenced by repeated reduction/reoxidation processes, as this combustion reaction follows the Mars van Krevelen (MvK) mechanism [2,12,21,23,29].

In this study, we therefore assumed that the above-mentioned phenomena are strongly related, as both originate from the reduction/reoxidation process and result in improved catalytic activities. Thus, we herein attempt to present experimental evidence demonstrating such a relationship through CH₄ temperature-programmed reduction (TPR) measurements. For this purpose, Pd/ZrO₂ catalysts are employed, and the catalyst calcination temperature is used as the main experimental variable. We expect that the obtained results can be applied as the fundamental foundation for the catalytic methane combustion process, especially for the activity and reaction mechanism at low temperatures.

2. Results and Discussion

Following preparation of the various catalysts, their crystal structures were determined by X-ray diffraction (XRD), as shown in Figure 1. It is well known that pure ZrO₂ can exist in cubic, monoclinic, and tetragonal phases [33–35], where the crystal structure is strongly dependent on the synthetic conditions employed [33]. In addition, tetragonal ZrO₂ can only be stabilized under suitable preparative conditions below 1100 °C, as monoclinic ZrO₂ is the most thermodynamically stable polymorph in this temperature range. In addition, Guo et al. [36–38] reported that as-synthesized tetragonal ZrO₂ can be transformed into monoclinic crystallites at relatively low temperatures (i.e., 65–400 °C), due to the presence of adsorbed hydroxyl groups originating from water molecules. In our previous work [35] this low-temperature degradation of the tetragonal species to monoclinic crystallites was also observed during Pd impregnation, as an aqueous Pd precursor solution was utilized for the impregnation process. More specifically, the portion of tetragonal crystallites in ZrO₂ exhibiting a mixed crystalline phase (i.e., both monoclinic and tetragonal) decreased following impregnation, while no changes were observed for the pure tetragonal ZrO₂. Like previous results, the support prepared herein exhibited a pure tetragonal crystalline phase (JCPDS No. 50-1089, see Figure 1), and this structure was maintained even following Pd impregnation regardless of the calcination temperature employed. This is likely due to the stabilizing effect of the small particle size [39–41] which results from higher aging temperatures and longer aging times compared to those employed in other studies [33,35]. More specifically, the formation of small particles likely results in increased Brunauer–Emmett–Teller (BET) surface areas, as discussed in the following paragraph.

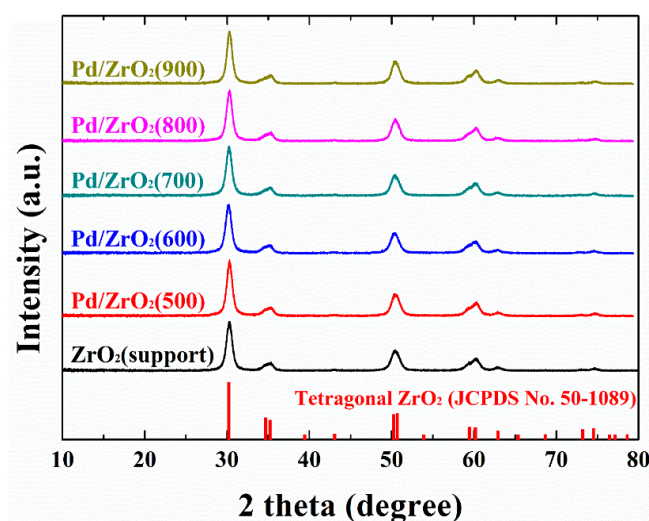


Figure 1. X-ray diffraction (XRD) patterns of the ZrO_2 support and the $\text{Pd/ZrO}_2(x)$ catalysts. The ZrO_2 support was pre-calcined at 900 °C for 6 h, then calcined at a range of different temperatures in Celsius degree (500–900 °C) following the impregnation of Pd.

Interestingly, no significant changes were observed in the ZrO_2 crystal size and the BET surface areas between the support and the impregnated catalysts, as indicated in Table 1. This is likely due to the high calcination temperature (900 °C) employed for treatment of the support. In addition, diffraction peaks corresponding to PdO and Pd were absent for all samples, indicating that the impregnated Pd species were either present in insufficient quantities (i.e., 1 wt.%) or were too highly dispersed (i.e., in the form of small crystallites) to be detected by XRD. It was therefore apparent that the results discussed in the following sections arise only from variations in the characteristics of the impregnated Pd species due to different calcination temperatures, with no significant variations in support characteristic. The dispersion and particle size of the impregnated Pd species were then calculated from the CO chemisorption measurements, with the results being largely influenced by the calcination temperature, as summarized in Table 1. More specifically, upon increasing the calcination temperature, the particle size gradually increased from 4.0 nm (at 500 °C) to 8.3 nm (800 °C) due to thermal sintering. A significant decrease in the metal dispersion was also observed at calcination temperatures >800 °C, which agrees with previously reported results [10,21]. We performed TEM analysis to confirm the presence of Pd nanoparticles. The size of tetragonal ZrO_2 particles used as support was very similar to that of Pd particles, making it very difficult to distinguish Pd particles (refer to TEM image in Figure S4).

Table 1. Physicochemical properties of the ZrO_2 support and the $\text{Pd/ZrO}_2(x)$ catalysts, as determined by XRD, CO chemisorption, and N_2 sorption measurements.

Sample	XRD	CO Chemisorption		N_2 Sorption		
	Crystal Size ^a (nm)	Pd Dispersion (%)	Pd Particle Size (nm)	S_{BET} ($\text{m}^2 \text{g}^{-1}$)	V_{P} ^b ($\text{cm}^3 \text{g}^{-1}$)	D_{P} ^c (nm)
ZrO_2 (support)	10.3	-	-	63	0.226	14.4
$\text{Pd/ZrO}_2(500)$	10.6	27.7	4.0	58	0.210	14.5
$\text{Pd/ZrO}_2(600)$	10.2	25.0	4.5	59	0.219	14.8
$\text{Pd/ZrO}_2(700)$	10.2	21.0	5.4	59	0.219	14.9
$\text{Pd/ZrO}_2(800)$	10.8	13.5	8.3	59	0.222	15.0
$\text{Pd/ZrO}_2(900)$	10.9	3.0	37.7	54	0.205	15.3

^a The crystal size was calculated by the Scherrer equation (Equation (1)) using the diffraction peak at $2\theta = 30.3^\circ$.

^b The total pore volume (V_{P}) was obtained from the volume of N_2 adsorbed at $P/P_0 = 0.995$ in the N_2 adsorption isotherm. ^c The average pore diameter (D_{P}) was calculated by the following formula: $(4 \times V_{\text{P}})/S_{\text{BET}}$.

The activation phenomenon was previously reported in various studies about methane combustion [6,8,11,20,21,30–32,35]. This phenomenon relates to an increase in methane conversion with increasing time-on-stream, and so it can be commonly detected from the results of isothermal reactions at defined reaction temperatures [6,8,20,21,30–32]. However, the activation phenomenon can also be observed by other methods. For example, Guerrero et al. [11] compared the results of conventional temperature-programmed (TP) reactions and stepwise TP reactions, where the temperature was maintained constant until a stable conversion was attained at each temperature, and they found that the conversion was improved due to activation at each temperature.

As shown in Figure 2, we herein performed the cyclic TP reaction over the Pd/ZrO₂(700) catalyst to examine the activation phenomenon. The methane conversions were higher in the second cycle than in the first cycle, which indicated that the catalytic activity improved as the reaction proceeded. In particular, the reaction of the second cycle was initiated at a lower temperature than that of the first cycle. This indicates that activation occurred through reduction/reoxidation processes during the first cycle, and that it led to an improved catalytic conversion and a lower light-off temperature (LOT) (i.e., the temperature at which the reaction is initiated). This was a similar result as that observed following pre-reduction. For example, Yang et al. [24] reported that a pre-reduced sample exhibited relatively low LOT and higher CH₄ conversion in the TP reaction. In addition, they noted that the initial state of the catalysts before contacting the reactant stream is important as the pre-reduced sample can be activated more rapidly. However, our results outlined in Figure 2 indicate that even without pre-reduction, the catalyst can transform to a more reactive phase through repeated reduction/reoxidation under the reactant stream. Furthermore, the conversions achieved during the third cycle were comparable to those of the second cycle, indicating that no significant decrease in catalytic activity was observed in the short reaction time interval of such cyclic TP reaction. The quantitative results obtained from the cyclic TP reaction (i.e., the T₅, T₅₀, and T₈₀ values) are summarized in Table S1.

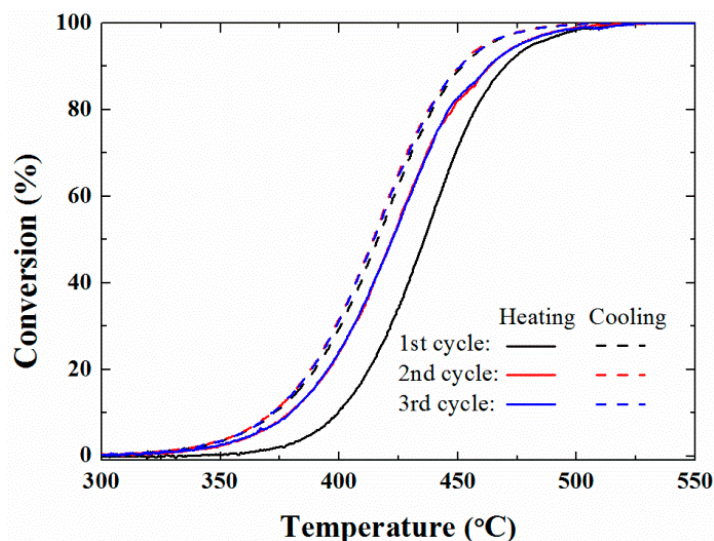


Figure 2. Methane conversions obtained from the cyclic temperature-programmed reactions of the Pd/ZrO₂(700) catalyst. The reaction was performed under a constant reactant composition of 10% H₂O/0.1% CH₄/3.15% O₂/N₂ balance with a total flow rate of 400 cm³/min (GHSV = 240,000 cm³ g cat⁻¹ h⁻¹). GHSV was defined as total flow rate of reactants (cm³ h⁻¹) per the weight of catalyst used (g catalyst).

Figure 3 shows the results of the TP reaction over the Pd/ZrO₂(x) catalysts both with and without activation periods. The quantitative results, outlined in Table 2 and obtained from Figure 3A (i.e., from the non-activated samples) indicated that the LOTs of the catalysts gradually shifted towards higher temperatures at higher calcination temperatures. However, as shown in Figure 3B, this tendency varied greatly following activation. As described in the experimental section, in the case of the activated reactions, the catalysts were pre-treated under the reaction stream for 1 h prior to commencement of

the TP reaction. Therefore, as outlined in Table 2, the temperatures at which conversions of 5%, 50%, and 80% were reached (i.e., T_5 , T_{50} , and T_{80}) were lower for all activated catalysts compared to the values recorded for the non-activated systems, with the exception of Pd/ZrO₂(900) catalyst. These results therefore demonstrate that repeated reduction/reoxidation through contact with the reactant stream can allow the catalytic combustion reaction to take place at lower temperatures. In addition, the degree of variation in the catalytic activity following the activation period was influenced by the calcination temperature. For example, the T_5 value over the Pd/ZrO₂(700) catalyst decreased from 384 to 365 °C, while that of the Pd/ZrO₂(900) catalyst increased from 411 to 443 °C following activation. Consequently, the LOTs of the activated catalysts exhibited a volcano-shaped curve as a function of the calcination temperature, with the lowest value being obtained for the Pd/ZrO₂(700) catalyst.

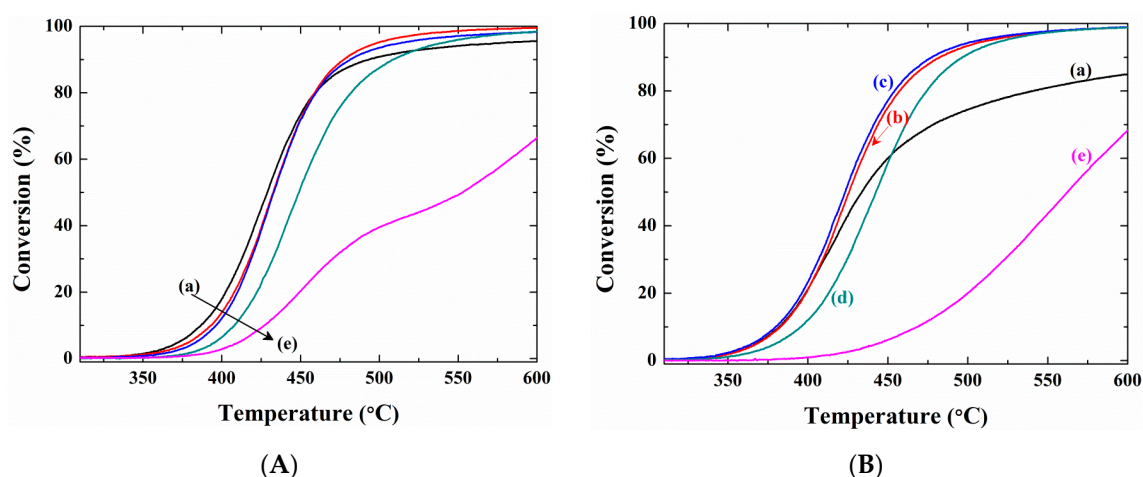


Figure 3. Temperature-programmed reactions over the Pd/ZrO₂(x) catalysts (A) without pretreatment, and (B) with pretreatment period: (a) Pd/ZrO₂(500); (b) Pd/ZrO₂(600); (c) Pd/ZrO₂(700); (d) Pd/ZrO₂(800); and (e) Pd/ZrO₂(900) catalysts. The reactant composition and the total flow rate were fixed as 10 vol.% H₂O/0.1% CH₄/3.15% O₂/N₂ balance and 400 cm³/min (GHSV = 240,000 cm³ g⁻¹ h⁻¹), respectively.

Table 2. Catalytic performances of the Pd/ZrO₂(x) catalysts obtained from the temperature-programmed reaction.

Sample	Without Activation ^a			With Activation ^a		
	T_5 (°C)	T_{50} (°C)	T_{80} (°C)	T_5 (°C)	T_{50} (°C)	T_{80} (°C)
Pd/ZrO ₂ (500)	373	429	460	368	434	541
Pd/ZrO ₂ (600)	380	433	460	368	426	467
Pd/ZrO ₂ (700)	384	433	460	365	424	449
Pd/ZrO ₂ (800)	396	450	482	380	443	474
Pd/ZrO ₂ (900)	411	553	-	443	562	-

^a T_X represents the temperature (°C) where a specific conversion, X%, was reached.

During the activation period, the catalysts were treated under the reaction stream at 500 °C for 1 h, and the methane conversion of the Pd/ZrO₂(x) catalysts during this period was also recorded, as indicated in Figure S2. Although the long-term stabilities of these catalysts could not be measured during this period, activation was successfully observed for all catalysts. Interestingly, significant deactivation was observed over the Pd/ZrO₂(900) catalyst, which was closely related to the increasing LOTs following the activation period, as indicated in Figure 3 and Table 2. On the other hand, the Pd/ZrO₂(600), Pd/ZrO₂(700), and Pd/ZrO₂(800) catalysts exhibited higher methane conversions during this period, and these catalysts gave lower LOTs after activation. These results therefore indicate that the reaction progress is associated with a decreasing LOT and improved catalytic activity, because the reduction/reoxidation occurred actively over these catalysts.

The key difference between Figures 2 and 3 relates to activation at a specific temperature range (i.e., in the range of 300–600 °C in Figure 2) or under isothermal conditions (i.e., at 500 °C in Figure 3). However, both experiments exhibited lower LOTs and improved catalytic activities, resulting from repeated reduction/reoxidation. For example, the T_5 , T_{50} , and T_{80} values of the Pd/ZrO₂(700) catalyst were comparable for both experiments, irrespective of the activation conditions employed (see Table 2 and Table S1). In addition, as previously mentioned in the TP reactions, the catalytic performances of the Pd/ZrO₂(x) catalysts following the activation period exhibited a volcano-shaped curve as a function of the calcination temperature. This tendency is in accordance with the methane conversion achieved under isothermal conditions, as indicated in Figure S2. It is therefore considered that the catalytic activity under isothermal conditions was dependent on the catalyst characteristics following the pretreatment period.

In general, precious and transition metals except Pd confirm the reducibility of the catalyst by H₂-TPR analysis. In the case of Pd catalysts, CH₄-TPR was often used to clarify the differentiation of the reduction levels because H₂ reduction can occur at a low temperature reduction below 30 °C. To reveal the origin of the activation phenomenon in this study, CH₄-TPR measurements were performed. Figure 4A shows the TPR profiles of the non-activated Pd/ZrO₂(x) catalysts, where all reduction peaks were observed between 200 and 425 °C. All reduction peaks could be deconvoluted into two distinct peaks, β and γ , which indicated that oxide species exhibiting different reduction behaviors were present on the support [42]. In addition, as shown in Table 3, the peak positions and relative portion of the peak area were influenced significantly by the calcination temperature. More specifically, the β and γ peak positions of the non-activated catalysts gradually shifted towards higher temperatures upon increasing the calcination temperature, and this tendency corresponded to that of the LOT (T_5 value) indicated in Figure 3A. Furthermore, the relative peak area portion of the β peak, which can be reduced more easily than the γ peak, decreased as the calcination temperature was increased. It was therefore apparent that the increased LOTs of the non-activated catalysts upon increasing the calcination temperature were directly related to changes in the catalyst reduction properties [42].

Table 3. Reduction temperature and relative portion of peak area obtained from the CH₄-TPR measurement over the non-activated and activated Pd/ZrO₂(x) catalysts.

Sample	Non-Activated			Activated		
	Peak Position (°C) (Relative Portion of Peak Area, %)			Peak Position (°C) (Relative Portion of Peak Area, %)		
	α	β	γ	α	β	γ
Pd/ZrO ₂ (500)	-	311(62)	332 (38)	277 (24)	297 (49)	316 (27)
Pd/ZrO ₂ (600)	-	313 (62)	332 (38)	274 (35)	293 (50)	314 (15)
Pd/ZrO ₂ (700)	-	321 (60)	337 (40)	271 (36)	289(47)	307 (17)
Pd/ZrO ₂ (800)	-	342 (60)	356 (40)	274 (34)	294 (50)	308 (16)
Pd/ZrO ₂ (900)	-	357 (34)	370 (66)	-	366 (84)	386 (16)

As indicated by the results presented in Figure 3, the catalytic performance varied significantly following activation, and so it could be expected that the reduction characteristics would also be affected by the activation process. Prior to deconvolution of the reduction peaks of the activated Pd/ZrO₂(x) catalysts, the peaks became broader and more intense than those of the non-activated catalysts. Thus, upon the deconvolution of these peaks using the same criterion (i.e., deconvolution into two peaks), the deconvoluted peaks exhibited a wider full width at half-maximum (FWHM) value of 35 °C, as shown in Figure S3. Furthermore, the reduction temperature of the Pd/ZrO₂ (800) catalyst was lower than that of the Pd/ZrO₂(600) catalyst, as summarized in Table S2. It is therefore not clear why the Pd/ZrO₂(600) catalyst exhibited a significantly lower LOT than the Pd/ZrO₂(800) catalyst following activation (Figure 3B). Thus, as shown in Figure 4B, the reduction peak should be deconvoluted into three different peaks (α , β , and γ), except for that of the activated Pd/ZrO₂(900) catalyst, which indicated

that a new reduction peak (α) was developed through repeated reduction/reoxidation during activation. Consequently, the reduction temperatures of the activated catalysts in the CH_4 -TPR measurements correlated with their LOTs, as shown in Figure 5. In addition, the relative peak area portion of the α peak area exhibited the same trend with that of reduction temperature, and thus the LOTs of the catalysts dropped as the reduction temperature decreased and the α peak area portion increased. Vedyagin et al. [43] reported that the shift of the bulk PdO reduction peak to low temperature in H_2 -TPR of Pd/ZrO₂ catalyst indicates a change in metal-support interaction. In this study, it was also found that the reduction of the Pd catalyst was increased through the reduction/reproduction processes from the shift of the peak at low temperature in the CH_4 -TPR analysis.

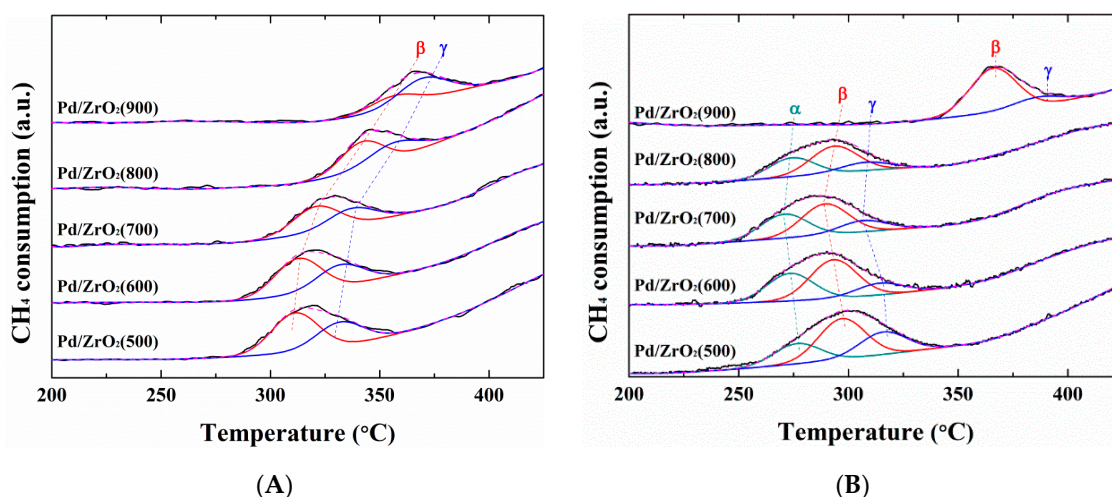


Figure 4. CH_4 -TPR (temperature-programed reduction) profiles of (A) the non-activated, and (B) activated Pd/ZrO₂(x) catalysts.

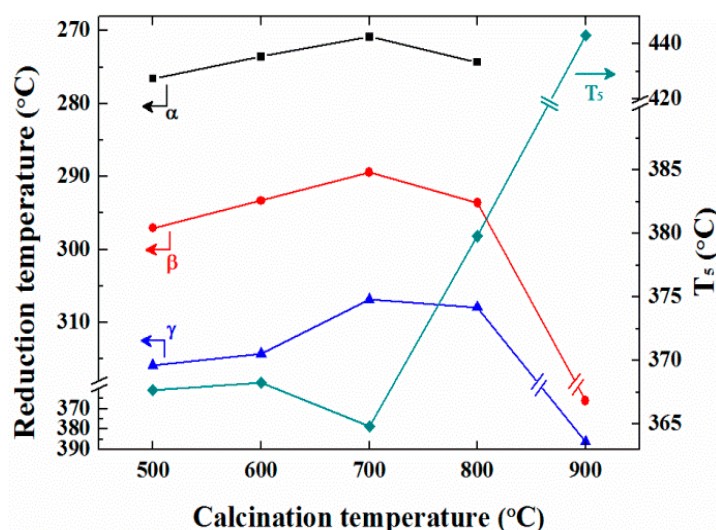


Figure 5. Correlation curves between the reduction temperatures and the T_5 values of the activated Pd/ZrO₂(x) catalysts. The reduction temperatures and the T_5 values of the activated Pd/ZrO₂(x) catalysts were obtained from the CH_4 -TPR and the temperature-programed reaction, respectively.

From the data presented in Figures 2 and 3, it was confirmed that the LOT values of the catalysts decreased upon repeated reduction/reoxidation during activation, which took place under the reactant stream regardless of the activation temperature. Monai et al. [28] reported interesting results regarding the combustion of methane over Pd@CeO₂/Si-Al₂O₃ catalysts. They found that the pre-reduced catalyst formed under flowing H₂ almost fully decomposed into Pd, while the reduced Pd species slowly

reformed the oxide species under a dry reactant stream, although the methane conversion increased rapidly to 100%. This result indicated that the reoxidized catalyst exhibited a higher catalytic activity, despite its low oxygen content. It is expected that this result may be closely related to our CH₄-TPR observations (Figure 4), in which the reduction properties varied upon contact with the reactant stream, and the new α reduction peak was detected following this activation process. In addition, the newly formed α species exhibited the lowest reduction temperature, thereby indicating its facile reduction and active participation in the methane combustion reaction. We therefore proposed a potential activation mechanism as outlined in Figure 6. It is well known that the mechanism for the methane combustion reaction follows the reduction-oxidation pathway of the Mars van Krevelen mechanism [2,12,21,23,29] with the first step being reduction of the as-formed lattice oxygen species (indicated as “O” in Figure 6) by methane. Subsequently, oxygen-vacant sites are refilled with oxygen from the reactant stream. From our observations in the CH₄-TPR measurements, the reactivity of this re-filled oxygen (indicated as “O*” in Figure 6) was higher than that of the as-formed oxygen, and thus the improved catalytic performance originates from repeated reduction/reoxidation processes. Although the difference in the oxygen state following activation cannot be demonstrated by x-ray photoelectron spectroscopy (XPS) analysis due to spectral overlap of the Pd 3d_{5/2} and Zr 3p_{3/2} spectra, it was expected that the newly developed species corresponded to PdO_x (0 < x < 1) or PdO_x adjacent to Pd⁰ species [24,44]. In addition to the role of Pd particles as well as the role of support zirconia, the reactivity may change due to non-stoichiometric oxides that can generate active oxygen. Müller et al. [12] reported that pre-reduction can improve the performance of the catalyst and that the initially oxidized catalyst has a strong interaction with the support. The active metal component, which has undergone the reduction/reoxidation process, has strong interaction with the support, and the interaction state changes the oxidation state of Pd. As a result, newly filled oxygen has been reported to have higher activity than the initial lattice oxygen.

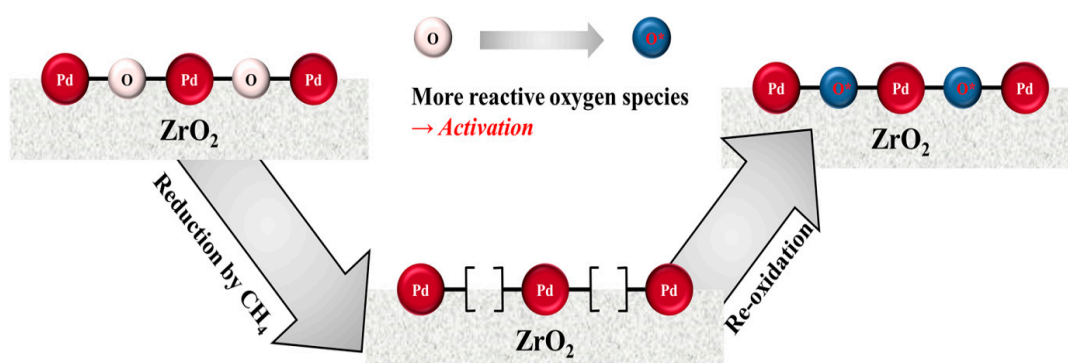


Figure 6. Schematic representation of activation phenomenon over the Pd/ZrO₂ catalysts through reduction/reoxidation during the methane combustion reaction.

Figure 7A shows the results of the isothermal reactions carried out over the Pd/ZrO₂(x) catalysts in the absence of water vapor at 400 °C for 15 h on stream. Under dry conditions, activation was observed for all catalysts in the initial stages of the reaction, which indicated that the activation phenomenon took place even in the absence of water vapor. It was also found that the catalytic activities of the Pd/ZrO₂(x) catalysts increased in the following order: Pd/ZrO₂(900) < Pd/ZrO₂(800) < Pd/ZrO₂(500) < Pd/ZrO₂(600) < Pd/ZrO₂(700). This trend corresponds with those of the TP reaction following activation (see Figure 3B), and of the isothermal reaction at 500 °C in the presence of 10% water vapor (see Figure S2). As a result, the catalytic activity appeared to be influenced largely by the calcination temperature, and a slight deactivation was observed for all catalysts, as outlined in Table 4. In addition, under wet conditions (see Figure 7B), the variation in the methane conversion as a function of the calcination temperature was identical to that observed under dry conditions, but the degree of deactivation was more pronounced (see Table 4). Although catalytic deactivation is known to be caused by the thermal decomposition of PdO to metallic Pd⁰ [8,22,23], and by the accumulation of hydroxyl groups originating from adsorbed

water molecules [5,13,26,27] we previously found that catalytic deactivation was prevented on Pd/ZrO₂ catalysts [35] with activation being observed only during combustion under identical reaction conditions compared to those employed herein (i.e., at 450 °C in the presence of 10% water vapor). We therefore assumed that deviations in the hydrothermal stability mainly resulted from the different calcination temperature of the ZrO₂ support (i.e., previous work: 600 °C [35] and this work: 900 °C), and so an additional catalyst was prepared using a different support calcination temperature.

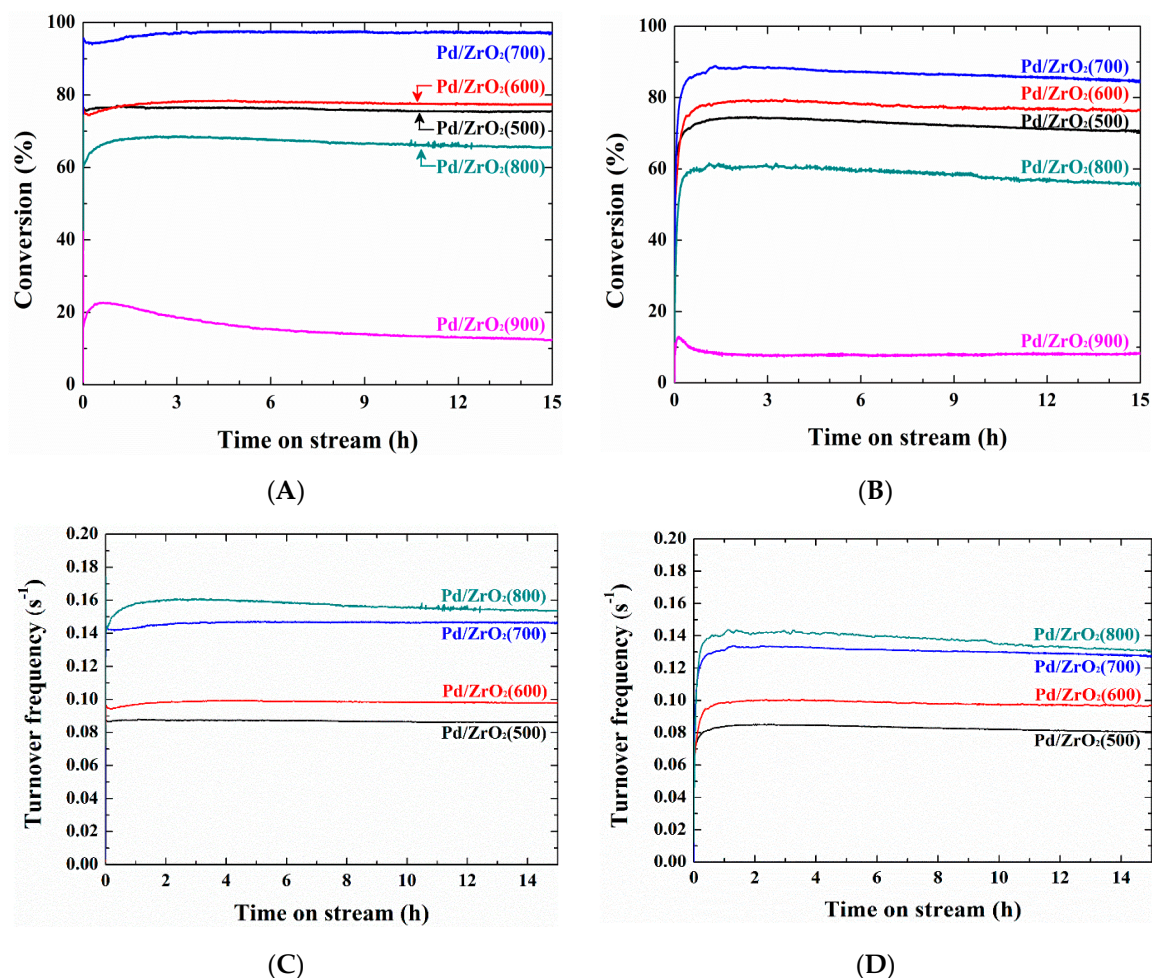


Figure 7. Isothermal reactions over the Pd/ZrO₂(x) catalysts: (A) conversion and (C) turnover frequency (TOF) in the absence of water vapor at 400 °C, and (B) conversion and (D) TOF in the presence of 10 vol% water vapor at 450 °C. The total flow rate was fixed at 400 cm³/min (GHSV = 240,000 cm³ g cat⁻¹ h⁻¹).

Table 4. Quantitative results from the isothermal reaction over the Pd/ZrO₂(x) catalysts.

Sample	Isothermal Reaction at 400 °C (Dry Conditions)			Isothermal Reaction at 450 °C (Wet Conditions)		
	X _{init} ^a (%)	X _{15h} ^b (%)	R _d ^c (%/h)	X _{init} ^a (%)	X _{15h} ^b (%)	R _d ^c (%/h)
Pd/ZrO ₂ (500)	76.7	75.5	0.10	75.9	70.5	0.47
Pd/ZrO ₂ (600)	78.8	77.3	0.13	80.8	76.0	0.40
Pd/ZrO ₂ (700)	97.6	97.2	0.03	89.7	84.6	0.38
Pd/ZrO ₂ (800)	40.0	35.6	0.73	62.7	55.7	0.74
Pd/ZrO ₂ (900)	24.8	12.4	3.33	24.0	8.2	4.39

^a X_{init} indicates the initial conversion obtained by extrapolation to an initial conversion. ^b X_{15h} is the conversion after 15 h on stream. ^c The deactivation rate (R_d) was calculated using the following expression: R_d = (X_{init} - X_{15h})/(X_{init}·15 h) × 100.

Turnover frequency (TOF) calculations are performed on the isotherm data (Figure 7C,D) to compare catalytic activity with various Pd particle sizes controlled by changes in calcination temperature. The Pd particle size obtained due to the sintering caused by the high calcination temperature of 900 °C was very high at 38 nm. For Pd/ZrO₂ catalysts excluding this sample, TOF increased with increasing Pd particle size from 4 to 8.3 nm (Table 1). Although this increase in Pd particle size was reported to be proportional to the catalyst activity [12], on the contrary it was reported that CH₄ combustion reaction over Pd catalyst is not sensitive which means that catalytic activity is not dependent on Pd particle size [45].

Figure 8 shows the evolution of methane conversion of the isothermal long-term reaction over the Pd/ZrO₂(900,700) and Pd/ZrO₂(700,700) catalysts at 450 °C in the presence of 10% water vapor. Interestingly, the methane conversion of the Pd/ZrO₂(700,700) catalyst was lower than that of the Pd/ZrO₂(900,700) catalyst, likely due to the relatively high BET surface area (153 m² g⁻¹) of the support in the Pd/ZrO₂(700,700) catalyst, which resulted in small PdO particles being formed on the surface. This occurs due to the larger PdO binding energy of the small particles, indicating that it is not easily reduced by methane [21,35]. In contrast, the Pd/ZrO₂(700,700) catalyst exhibited a stable performance for 100 h ($R_d = 0.11\%/h$), which was considered to result mainly from the low calcination temperature of the support, although it may also be related to the mobility of lattice oxygen in the ZrO₂ matrix [46]. Although the relationship between the oxygen mobility and the hydrothermal stability has only been touched upon herein, we consider it worthy of further investigation.

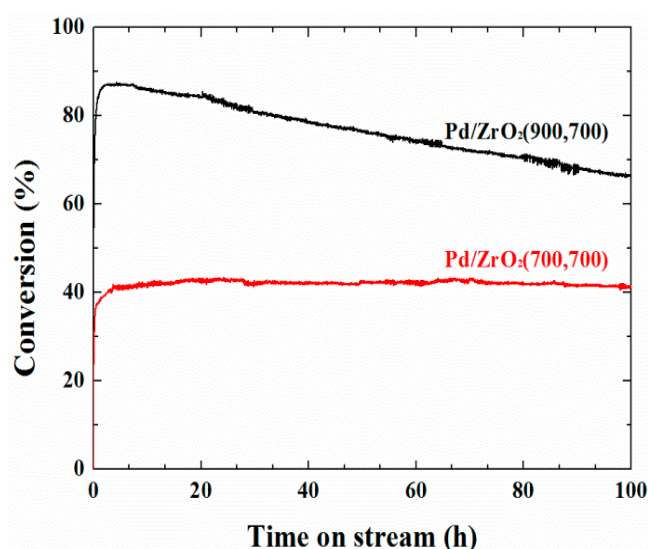


Figure 8. The long-term stability of the Pd/ZrO₂(900,700) and Pd/ZrO₂(700,700) catalysts at 450 °C under the wet conditions. The reaction was performed under a constant reactant composition of 10% H₂O/0.1% CH₄/3.15% O₂/N₂ balance with a total flow rate of 400 cm³/min (GHSV = 240,000 cm³ g cat⁻¹ h⁻¹).

Figure 8 shows the evolution of methane conversion of the isothermal long-term reaction over the Pd/ZrO₂(900,700) and Pd/ZrO₂(700,700) catalysts at 450 °C in the presence of 10 vol% water vapor. Interestingly, the methane conversion of the Pd/ZrO₂(700,700) catalyst was lower than that of the Pd/ZrO₂(900,700) catalyst, likely due to the relatively high BET surface area (153 m² g⁻¹) of the support in the Pd/ZrO₂(700,700) catalyst, which resulted in small PdO particles being formed on the surface. This occurs due to the larger PdO binding energy of the small particles, indicating that it is not easily reduced by methane [21,35]. In contrast, the Pd/ZrO₂(700,700) catalyst exhibited a stable performance for 100 h ($R_d = 0.11\%/h$), which was considered to result mainly from the low calcination temperature of the support, although it may also be related to the mobility of lattice oxygen in the ZrO₂ matrix [46]. Although the relationship between the oxygen mobility and the hydrothermal stability has only been touched upon herein, we consider that it is worthy of further investigation.

3. Experimental

3.1. Catalyst Preparation

The ZrO₂ support was synthesized via a chemical precipitation method using ZrO(NO₃)₂·2H₂O (99%, KANTO, Japan) and NH₄OH (28 wt.%, SK Chemical, Korea) as the precursor and the precipitant, respectively. A 2 wt.% NH₄OH solution was then added dropwise to the 0.5 M zirconium oxynitrate precursor solution until a pH of 9.5 was reached. Subsequently, the resulting solution was aged at 100 °C for 72 h, and the reactor was fitted with a reflux condenser to prevent solvent loss during the aging procedure. The obtained precipitate was then filtered, washed with deionized water, dried at 60 °C overnight, and then calcined at 900 °C for 6 h under a flow of air. The 1 wt.% Pd/ZrO₂ catalyst was prepared via an incipient wetness impregnation method using a 10 wt.% solution of Pd(NO₃)₂. The impregnated catalyst was dried at 60 °C for 24 h, and then calcined at a desired temperature between 500 and 900 °C for 2 h. The obtained catalysts were labeled as Pd/ZrO₂(x), where x indicates the calcination temperature in degrees Celsius following the impregnation of Pd. As the calcination temperature of the support in Pd/ZrO₂(x) was equal to 900 °C, it was omitted for ordinary cases mentioned above. However, in the case of the Pd/ZrO₂(700,700) catalyst synthesized to confirm the effect of the support calcination temperature, the first and second values in parentheses represent the calcination temperatures of the support and the impregnated catalyst, respectively.

3.2. Characterization

To identify the crystalline structures of the samples, X-ray diffraction (XRD) measurements were carried out on a D8 Discover with a GADDS X-ray diffractometer (Bruker AXS, USA) using Cu K α radiation (scan size = 0.01°/step, and scan rate = 0.2 s/step). From the obtained XRD patterns, the crystallite size (D, nm) was calculated using the Scherrer equation (Equation (1)):

$$D = K\lambda/\beta\cos\theta \quad (1)$$

where K is the shape factor of the particle (0.89), λ is the X-ray wavelength (0.15406 nm), β is the corrected FWHM in radian, and θ is the Bragg diffraction angle in degrees. To measure the degree of CO chemisorption on the supported Pd species, volumetric CO chemisorption measurements were conducted using an Autochem II 2920 (Micromeritics, USA). Prior to analysis, the catalyst was reduced under H₂ flow for 1 h at 200 °C. The adsorption measurements were then performed at 100 °C, and the dispersion and particle size were calculated from the total CO uptake by assuming a stoichiometry of CO/Pd = 1. To estimate the BET surface areas, total pore volumes, and average pore diameters of the samples, N₂-sorption isotherms were measured using a Micromeritics ASAP 2020 (USA). Prior to measurement, the samples were degassed under a vacuum for 5 h at 250 °C.

The reduction characteristics of the supported PdO species were investigated by CH₄-TPR measurements using a sample mass of 0.1 g. For the purpose of the CH₄-TPR measurements, the experimental conditions were categorized into non-activated and activated experiments, depending on the pretreatment conditions employed. As shown in Figure 9, pretreatment at 500 °C for 1 h under a flow of air (50 cm³/min) was carried out in all cases, and the non-activated CH₄-TPR experiments were conducted without any additional treatment. In contrast, for the activated CH₄-TPR experiments, further treatment was carried out at 500 °C for 1 h under a stream of the reactant in the presence of 10% water vapor (10% H₂O/0.1% CH₄/3.15% O₂/N₂ balance in volume, and total flow rate = 400 cm³/min). This additional treatment was termed the activation period. Following this activation period, the sample was cooled to 150 °C under a flow of air, then heated to 500 °C with a heating rate of 5 °C/min under 0.5% CH₄/N₂ (total flow rate = 30 cm³/min). The quantity of CH₄ consumed was analyzed using an infrared gas analyzer (Model 7500, Teledyne Analytical Instruments, CA, USA).

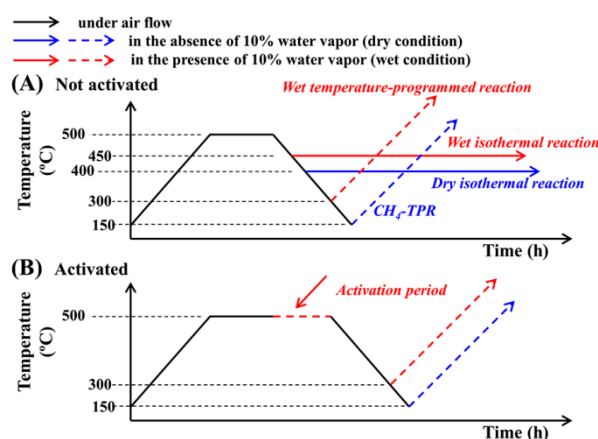


Figure 9. Experimental procedures of CH₄-TPR and CH₄ combustion reaction for (A) the non-activated and (B) activated sample.

3.3. Methane Combustion Reaction

For the temperature-programmed or isothermal methane combustion reaction, the 1 wt.% Pd/ZrO₂ catalyst (0.1 g) was loaded into a quartz fixed bed reactor (I.D. 12 mm). The reactant composition was fixed at 0.1% CH₄/3.15% O₂/N₂ balance with a total flow rate of 400 cm³/min (GHSV = 240,000 cm³ g⁻¹ h⁻¹) in either the presence or absence of 10 vol% water vapor. GHSV was defined as total flow rate of reactants (cm³ h⁻¹) per the weight of catalyst used (g catalyst).

During the reaction, the CH₄ concentration was measured using an infrared gas analyzer (Model 7500, Teledyne Analytical Instruments, CA, USA), and the CH₄ conversion was calculated according to Equation (2):

$$\text{CH}_4 \text{ conversion } (X, \%) = \frac{\text{CH}_4 \text{ in} - \text{CH}_4 \text{ out}}{\text{CH}_4 \text{ in}} \times 100 \quad (2)$$

where CH_{4 in} and CH_{4 out} are the molar flow rates of CH₄ at the inlet and outlet, respectively.

Turnover frequency (TOF, s⁻¹) was defined as the molecule of CH₄ reacted per molecules of Pd particles exposed per second.

A non-activated sample means that pretreatment was done at 500 °C for 1 h under air flowing (50 cm³/min). Activation comprehends air pretreatment at 500 °C for 1 h and subsequently maintains for 1 h in CH₄ combustion conditions with 0.1% CH₄/3.15% O₂/N₂ balance with a total flow rate of 400 cm³/min (GHSV = 240,000 cm³ g⁻¹ h⁻¹) in the presence of 10 vol% water vapor. The experimental procedure of CH₄-TPR and CH₄ combustion reaction for the non-activated and activated sample of Pd/ZrO₂ catalyst either in the presence of absence of 10 vol% H₂O vapor is summarized in Figure 9.

3.3.1. Temperature-Programmed (TP) Reaction

Prior to the temperature-programmed reaction, pretreatment was carried out at 500 °C under air flow (50 cm³/min) for 1 h. Following pretreatment, the TP reaction of the non-activated catalyst was conducted in the presence of 10% water vapor at temperatures ranging from 300 to 600 °C with a heating rate of 5 °C/min. Similar to the above-mentioned CH₄-TPR measurements, the activated TP reaction was carried out following the activation period. For the cyclic TP reaction, the reactor was heated and cooled with a rate of 5 °C/min in the temperature range of 300–600 °C, and the heating and cooling cycles were repeated three times. From the result of the TP reaction, the LOT was defined as the temperature where a methane conversion of 5% was reached (T₅).

3.3.2. Isothermal Reaction

For the isothermal reaction, the pretreatment conditions and the reactant composition were the same with the TP reaction mentioned above. The isothermal reactions were performed for 15 h in the presence and absence of 10 vol.% water vapor at 400 and 450 °C, respectively. For testing the long-term

stability, the isothermal reaction was conducted in the presence of 10 vol.% water vapor for 100 h at 450 °C.

4. Conclusions

We herein report the catalytic activity of Pd/ZrO₂(x) catalysts treated at different calcination temperatures (i.e., 500–900 °C), and subsequent phenomenon investigation of their catalytic performances in the methane combustion reaction. It was found that in the cyclic TP reaction, the catalytic activities of the second and third cycles were superior to that of the first cycle. In particular, the reaction was initiated at lower temperatures as the number of cycles proceeded. This activation phenomenon was also observed in the TP reaction of activated Pd/ZrO₂(x) catalysts, which were pretreated under the reactant stream for 1 h prior to starting the reaction. To reveal the origin of activation, the CH₄-TPR was performed, and it was found that the improved activity and lower light-off temperature (LOT) were closely related to variations in the reduction properties through repeated reduction/reoxidation during activation. In addition, the catalytic activities of the Pd/ZrO₂(x) catalysts exhibited a volcano-shaped curve as a function of the calcination temperature in the isothermal reaction, and the samples exhibiting higher activities had lower LOTs in the TP reaction following activation. The increase in Pd particle size in the range from 4–8.3 nm could be related to the catalytic activity calculated by TOF. It can therefore be concluded that the as-formed oxygen species on the palladium were converted into more reactive species through repeated reduction/reoxidation cycles under the reactant stream.

Supplementary Materials: The following are available online at <http://www.mdpi.com/2073-4344/9/10/838/s1>. Figure S1: N₂-sorption isotherms of ZrO₂ support and Pd/ZrO₂(x) catalysts. X in parentheses means calcination temperature in degrees Celsius, Figure S2: Methane conversion of Pd/ZrO₂(x) catalysts during activation period at 500 °C for 1 h, Figure S3: CH₄-TPR profiles of activated Pd/ZrO₂(x) catalysts being deconvoluted into two different reduction peaks, Figure S4: TEM image of the Pd/ZrO₂(700) catalyst, Table S1: The quantitative results obtained from cyclic temperature-programmed reactions over Pd/ZrO₂(700) catalyst, Table S2: Quantitative results calculated from CH₄-TPR over activated Pd/ZrO₂(x) catalysts in Figure S3.

Author Contributions: Conceptualization, E.H. and C.-H.S.; methodology, C.K., E.H., and C.-H.S.; formal analysis, C.K., E.H., and C.-H.S.; investigation C.K., E.H., and C.-H.S.; resources, C.K. and C.-H.S.; data curation, C.K.; writing—original draft preparation, C.K. and E.H.; writing—review and editing, C.K., E.H., and C.-H.S.; supervision, C.-H.S.; project administration, E.H. and C.-H.S.; funding acquisition, C.-H.S.

Funding: This research was supported by the Basic Science Research Program through the National Research Foundation of Korea (NRF) funded by the Ministry of Science, ICT, and Future Planning (2017R1A2B3011316).

Acknowledgments: This research was supported by Basic Science Research Program through the National Research Foundation of Korea (NRF) funded by the Ministry of Science, ICT, and Future Planning (2017R1A2B3011316).

Conflicts of Interest: The authors declare no conflicts of interest.

References

1. Liu, Y.; Wang, S.; Sun, T.; Gao, D.; Zhang, C.; Wang, S. Enhanced hydrothermal stability of high performance lean fuel combustion alumina-supported palladium catalyst modified by nickel. *Appl. Catal. B Environ.* **2012**, *119–120*, 321–328. [[CrossRef](#)]
2. Yang, L.; Shi, C.; He, X.; Cai, J. Catalytic combustion of methane over PdO supported on Mg-modified alumina. *Appl. Catal. B Environ.* **2002**, *38*, 117–125. [[CrossRef](#)]
3. Marti, P.; Maciejewski, M.; Baiker, A. Methane combustion over La_{0.8}Sr_{0.2}MnO_{3+x} supported on MA₂O₄ (M = Mg, Ni and Co) spinels. *Appl. Catal. B Environ.* **1994**, *4*, 225–235. [[CrossRef](#)]
4. Liotta, L.F.; Di Carlo, G.; Pantaleo, G.; Deganello, G. Co₃O₄/CeO₂ and Co₃O₄/CeO₂-ZrO₂ composite catalysts for methane combustion: Correlation between morphology reduction properties and catalytic activity. *Catal. Commun.* **2005**, *6*, 329–336. [[CrossRef](#)]
5. Liu, Y.; Wang, S.; Gao, D.; Sun, T.; Zhang, C.; Wang, S. Influence of metal oxides on the performance of Pd/Al₂O₃ catalysts for methane combustion under lean-fuel conditions. *Fuel Process. Technol.* **2013**, *111*, 55–61. [[CrossRef](#)]
6. Demoulin, O.; Ruppel, G.; Seunier, I.; Le Clef, B.; Navez, M.; Ruiz, P. Investigation of Parameters Influencing the Activation of a Pd/γ-Alumina Catalyst during Methane Combustion. *J. Phys. Chem. B* **2005**, *109*, 20454–20462. [[CrossRef](#)] [[PubMed](#)]

7. Kinnunen, N.M.; Hirvi, J.T.; Kallinen, K.; Maunula, T.; Keenan, M.; Suvanto, M. Case study of a modern lean-burn methane combustion catalyst for automotive applications: What are the deactivation and regeneration mechanisms? *Appl. Catal. B Environ.* **2017**, *207*, 114–119. [[CrossRef](#)]
8. Lyubovsky, M.; Pfefferle, L. Methane combustion over the α -alumina supported Pd catalyst: Activity of the mixed Pd/PdO state. *Appl. Catal. A Gen.* **1998**, *173*, 107–119. [[CrossRef](#)]
9. Huang, K.; Wang, L.; Xu, Y.; Wu, D. Novel multi-scale diffusion model for catalytic methane combustion. *Korean J. Chem. Eng.* **2017**, *34*, 1366–1376. [[CrossRef](#)]
10. Narui, K.; Furuta, K.; Yata, H.; Nishida, A.; Kohtoku, Y.; Matsuzaki, T. Catalytic activity of PdO/ZrO₂ catalyst for methane combustion. *Catal. Today* **1998**, *45*, 173–178. [[CrossRef](#)]
11. Guerrero, S.; Araya, P.; Wolf, E.E. Methane oxidation on Pd supported on high area zirconia catalysts. *Appl. Catal. A Gen.* **2006**, *298*, 243–253. [[CrossRef](#)]
12. Müller, C.A.; Maciejewski, M.; Koepfel, R.A.; Baiker, A. Combustion of methane over palladium/zirconia: Effect of Pd-particle size and role of lattice oxygen. *Catal. Today* **1999**, *47*, 245–252. [[CrossRef](#)]
13. Park, J.H.; Cho, J.H.; Kim, J.Y.; Kim, E.S.; Han, H.S.; Shin, C.-H. Hydrothermal stability of Pd/ZrO₂ catalysts for high temperature methane combustion. *Appl. Catal. B Environ.* **2014**, *160–161*, 135–143. [[CrossRef](#)]
14. Guillaume, N.; Primet, M. Catalytic combustion of methane: Copper oxide supported on high-specific-area spinels synthesized by a sol-gel process. *J. Chem. Soc. Faraday Trans.* **1994**, *90*, 1541–1545. [[CrossRef](#)]
15. Pan, X.; Zhang, Y.; Miao, Z.; Yang, X. A novel PdNi/Al₂O₃ catalyst prepared by galvanic deposition for low temperature methane combustion. *J. Energy Chem.* **2013**, *22*, 610–616. [[CrossRef](#)]
16. Takeguchi, T.; Takeoh, O.; Aoyama, S.; Ueda, J.; Kikuchi, R.; Eguchi, K. Strong chemical interaction between PdO and SnO₂ and the influence on catalytic combustion of methane. *Appl. Catal. A Gen.* **2003**, *252*, 205–214. [[CrossRef](#)]
17. Grunwaldt, J.D.; Maciejewski, M.; Baiker, A. In situ X-ray absorption study during methane combustion over Pd/ZrO₂ catalysts. *Phys. Chem. Chem. Phys.* **2003**, *5*, 1481–1488. [[CrossRef](#)]
18. Müller, C.A.; Koepfel, R.; Maciejewski, M.; Heveling, J.; Baiker, A. Methane combustion over catalysts prepared by oxidation of ternary Pd₁₅x10Zr₇₅ (X = Co, Cr, Cu, Mn and Ni) amorphous alloys. *Appl. Catal. A Gen.* **1996**, *145*, 335–349. [[CrossRef](#)]
19. Dai, Q.; Bai, S.; Lou, Y.; Wang, X.; Guo, Y.; Lu, G. Sandwich-like PdO/CeO₂ nanosheet@HZSM-5 membrane hybrid composite for methane combustion: Self-redispersion, sintering-resistance and oxygen, water-tolerance. *Nanoscale* **2016**, *8*, 9621–9628. [[CrossRef](#)]
20. Burch, R.; Urbano, F. Investigation of the active state of supported palladium catalysts in the combustion of methane. *Appl. Catal. A Gen.* **1995**, *124*, 121–138. [[CrossRef](#)]
21. Fujimoto, K.; Ribeiro, F.H.; Avalos-Borja, M.; Iglesia, E. Structure and Reactivity of PdO_x/ZrO₂ Catalysts for Methane Oxidation at Low Temperatures. *J. Catal.* **1998**, *179*, 431–442. [[CrossRef](#)]
22. Colussi, S.; de Leitenburg, C.; Dolcetti, G.; Trovarelli, A. The role of rare earth oxides as promoters and stabilizers in combustion catalysts. *J. Alloys Compd.* **2004**, *374*, 387–392. [[CrossRef](#)]
23. Yin, F.; Ji, S.; Wu, P.; Zhao, F.; Li, C. Deactivation behavior of Pd-based SBA-15 mesoporous silica catalysts for the catalytic combustion of methane. *J. Catal.* **2008**, *257*, 108–116. [[CrossRef](#)]
24. Yang, S.; Maroto-Valiente, A.; Benito-Gonzalez, M.; Rodriguez-Ramos, I.; Guerrero-Ruiz, A. Methane combustion over supported palladium catalysts: I. Reactivity and active phase. *Appl. Catal. B Environ.* **2000**, *28*, 223–233. [[CrossRef](#)]
25. Park, J.H.; Ahn, J.H.; Sim, H.I.; Seo, G.; Han, H.S.; Shin, C.-H. Low-temperature combustion of methane using PdO/Al₂O₃ catalyst: Influence of crystalline phase of Al₂O₃ support. *Catal. Commun.* **2014**, *56*, 157–163. [[CrossRef](#)]
26. Persson, K.; Pfefferle, L.D.; Schwartz, W.; Ersson, A.; Järås, S.G. Stability of palladium-based catalysts during catalytic combustion of methane: The influence of water. *Appl. Catal. B Environ.* **2007**, *74*, 242–250. [[CrossRef](#)]
27. Burch, R.; Urbano, F.; Loader, P. Methane combustion over palladium catalysts: The effect of carbon dioxide and water on activity. *Appl. Catal. A Gen.* **1995**, *123*, 173–184. [[CrossRef](#)]
28. Monai, M.; Montini, T.; Chen, C.; Fonda, E.; Gorte, R.J.; Fornasiero, P. Methane Catalytic Combustion over Hierarchical Pd@CeO₂/Si-Al₂O₃: Effect of the Presence of Water. *ChemCatChem* **2015**, *7*, 2038–2046. [[CrossRef](#)]
29. Ciuparu, D.; Pfefferle, L. Contributions of lattice oxygen to the overall oxygen balance during methane combustion over PdO-based catalysts. *Catal. Today* **2002**, *77*, 167–179. [[CrossRef](#)]

30. Ribeiro, F.; Chow, M.; Dallabetta, R. Kinetics of the Complete Oxidation of Methane over Supported Palladium Catalysts. *J. Catal.* **1994**, *146*, 537–544. [[CrossRef](#)]
31. Baldwin, T.; Burch, R. Catalytic combustion of methane over supported palladium catalysts: I. Alumina supported catalysts. *Appl. Catal.* **1990**, *66*, 337–358. [[CrossRef](#)]
32. Briot, P.; Primet, M. Catalytic oxidation of methane over palladium supported on alumina: Effect of aging under reactants. *Appl. Catal.* **1991**, *68*, 301–314. [[CrossRef](#)]
33. Hong, E.; Baek, S.W.; Shin, M.; Suh, Y.W.; Shin, C.-H. Effect of aging temperature during refluxing on the textural and surface acidic properties of zirconia catalysts. *J. Ind. Eng. Chem.* **2017**, *54*, 137–145. [[CrossRef](#)]
34. Chuah, G.; Jaenicke, S. The preparation of high surface area zirconia—Influence of precipitating agent and digestion. *Appl. Catal. A Gen.* **1997**, *163*, 261–273. [[CrossRef](#)]
35. Hong, E.; Kim, C.; Lim, D.H.; Cho, H.J.; Shin, C.-H. Catalytic methane combustion over Pd/ZrO₂ catalysts: Effects of crystalline structure and textural properties. *Appl. Catal. B Environ.* **2018**, *232*, 544–552. [[CrossRef](#)]
36. Guo, X. On the degradation of zirconia ceramics during low-temperature annealing in water or water vapor. *J. Phys. Chem. Solids* **1999**, *60*, 539–546. [[CrossRef](#)]
37. Guo, X. Low temperature degradation mechanism of tetragonal zirconia ceramics in water: Role of oxygen vacancies. *Solid State Ion.* **1998**, *112*, 113–116. [[CrossRef](#)]
38. Guo, X. Property degradation of tetragonal zirconia induced by low-temperature defect reaction with water molecules. *Chem. Mater.* **2004**, *16*, 3988–3994. [[CrossRef](#)]
39. Garvie, R.C.; Goss, M.F. Intrinsic size dependence of the phase transformation temperature in zirconia microcrystals. *J. Mater. Sci.* **1986**, *21*, 1253–1257. [[CrossRef](#)]
40. Garvie, R.C. The occurrence of metastable tetragonal zirconia as a crystallite size effect. *J. Phys. Chem.* **1965**, *69*, 1238–1243. [[CrossRef](#)]
41. Garvie, R.C. Stabilization of the tetragonal structure in zirconia microcrystals. *J. Phys. Chem.* **1978**, *82*, 218–224. [[CrossRef](#)]
42. Shi, C.; Yang, L.; Wang, Z.; He, X.; Cai, J.; Li, G.; Wang, X. Promotion effects of ZrO₂ on the Pd/HZSM-5 catalyst for low-temperature catalytic combustion of methane. *Appl. Catal. A Gen.* **2003**, *243*, 379–388. [[CrossRef](#)]
43. Vedyagin, A.A.; Volodin, A.M.; Kenzhin, R.M.; Chesnokov, V.V.; Mishakov, I.V. CO oxidation over Pd/ZrO₂ Catalysts: Role of Support's Donor Sites. *Molecules* **2016**, *21*, 1289. [[CrossRef](#)] [[PubMed](#)]
44. Baylet, A.; Marecot, P.; Duprez, D.; Castellazzi, P.; Groppi, G.; Forzatti, P. In situ Raman and in situ XRD analysis of PdO reduction and Pd⁰ oxidation supported on γ -Al₂O₃ catalyst under different atmospheres. *Phys. Chem. Chem. Phys.* **2011**, *13*, 4607–4613. [[CrossRef](#)] [[PubMed](#)]
45. Zhu, G.; Han, J.; Zemlyanov, D.Y.; Ribeiro, F.H. The Turnover Rate for the Catalytic Combustion of Methane over Palladium Is Not Sensitive to the Structure of the Catalyst. *J. Am. Chem. Soc.* **2004**, *126*, 9896–9897. [[CrossRef](#)]
46. Choudhary, V.R.; Uphade, B.S.; Pataskar, S.G.; Keshavaraja, A. Low-Temperature Complete Combustion of Methane over Mn-, Co-, and Fe-Stabilized ZrO₂. *Angew. Chem. Int. Ed. Eng.* **1996**, *35*, 2393–2395. [[CrossRef](#)]

